

Hadron-nucleus elastic scattering at 70, 125, and 175 GeV/c

A. Schiz,* L. A. Fajardo, R. Majka,[†] J. N. Marx,[†] P. Némethy,[†] L. Rosselet,[‡] J. Sandweiss, and A. J. Slaughter
Yale University, New Haven, Connecticut 06520

C. Ankenbrandt, M. Atac, R. Brown,[§] S. Ecklund,^{||} P. J. Gollon,^{||} J. Lach, J. MacLachlan, A. Roberts, and
 G. Shen**

Fermi National Accelerator Laboratory, Batavia, Illinois 60510

(Received 19 November 1979)

Hadron-nucleus elastic scattering is measured for π^\pm , K^\pm , p , and \bar{p} scattering from Be, C, Al, Cu, Sn, and Pb targets at incident beam momenta of 70 and 175 GeV/c and for π^+ , K^+ , and p scattering from Be, Al, and Pb targets at an incident beam momentum of 125 GeV/c. Parametrizations of $d\sigma/dt$ in the forward direction for the reactions are presented.

I. INTRODUCTION

A measurement of hadron-nucleus elastic scattering is a fundamental one for any accelerator energy regime. In addition to testing theoretical approaches^{1,2} to the scattering process, the data also provide valuable technical information that aid in the design of high-energy physics experiments. In this experiment the elastic-scattering data include both interactions which leave the target nucleus in its ground state (coherent elastic scattering) and interactions which excite or break up the target nucleus (quasielastic scattering).

While data exist for hadron-nucleus elastic scattering at 20–30 GeV (Refs. 3 and 4) and at 40 GeV,⁵ we know of no comparable published measurements at higher energies for nuclear targets heavier than helium.⁶ We have performed an experiment at Fermilab where we measured the distribution in t , the square of the four-momentum transfer between the incident and forward scattered particle, for hadron-nucleus elastic scattering. Specifically, we studied π^\pm , K^\pm , p , and \bar{p} scattering from Be, C, Al, Cu, Sn, and Pb targets at incident beam momenta of 70 and 175 GeV/c and π^+ , K^+ , and p scattering from Be, Al, and Pb targets at an incident beam momentum of 125 GeV/c. The t range covered varied with the incident momentum. In all cases the minimum $-t$ is 0.001 (GeV/c)²; the maximum $-t$ is 0.05, 0.15, and 0.25 (GeV/c)² for incident beam momenta of 70, 125, and 175 GeV/c, respectively.

We present parametrizations of $d\sigma/dt$ in the very forward t region [$0.001 < -t < 0.030$ (GeV/c)²]. Hadron-nucleus elastic scattering is concentrated in the forward direction; therefore this forward t region represents the bulk of the elastic-scattering cross section. This is especially true as the atomic number of the nuclear target increases.

II. APPARATUS

The experiment was performed in the M6 West beam line⁷ at Fermilab. The apparatus, shown in Fig. 1, is a high-resolution single-arm spectrometer looking in the forward direction. The apparatus is described in detail in Refs. 8 and 9; therefore this section reviews only the salient features.

The incident beam momentum was measured with a precision of 0.05% ($\Delta p/p; \sigma$), with a systematic uncertainty of $\pm 0.25\%$. The beam line was instrumented with four Čerenkov counters which allowed simultaneous identification of pions, kaons, and protons. Electrons and muons, a small fraction of the beam, were tagged at the downstream end of the experiment.

The detectors which were used to measure the scattering angle and the nuclear target were mounted on a large reinforced concrete block to ensure stability. The targets were placed in identical holders and precisely positioned in an evacuated pipe. This design allowed easy substitution of targets. Table I presents the properties of each nuclear target. At the upstream end of the concrete block were beam-defining scintillation counters, $B1$ and $B2$, and a hole veto, $VH1$. Immediately downstream of the target were two scintillation counters, $VH2$ and $VH3$, used to suppress unwanted scatters from target electrons and hadronic inelastic scatters.

Two stations of high-resolution, high-pressure proportional wire chambers (PWC's)¹⁰ on either side of the nuclear target (stations 1–4 in Fig. 1) measured the scattering angle. At each station a measurement was made of the trajectory's x (horizontal) and y (vertical) coordinate. In addition, station 3 also measured the u and v coordinate (rotated 45 and 135 degrees from the horizontal). The chambers had a 70- μ m resolution

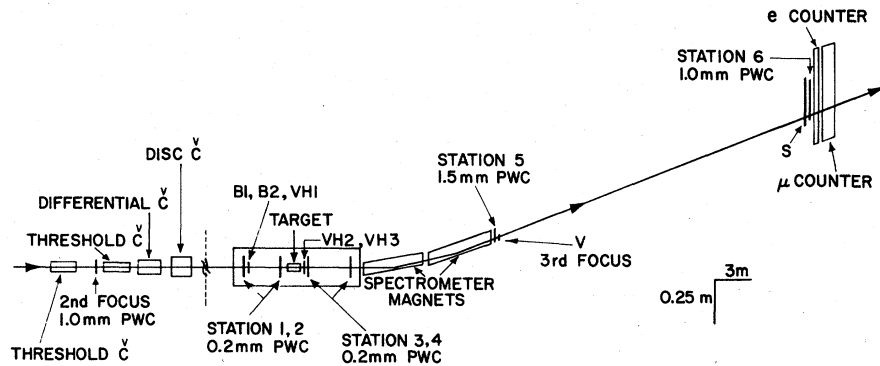


FIG. 1. Experimental apparatus (not to scale left of vertical dashed line).

(σ) and measured the scattering angle to an accuracy of $30 \mu\text{rad}$ (σ).

The spectrometer magnets used to determine the momentum of the scattered particle were two dipoles of the type used in the Fermilab main ring. Measurements of the integrated field length were made over the magnet aperture; these were uniform to 0.04%. A particle of the central momentum was bent 34 mrad in the horizontal plane. Using station 6 (a pair of PWC's with an effective wire spacing of 1 mm) in conjunction with stations 3 and 4, the outgoing momentum was measured to a precision of 0.1% ($\Delta p/p; \sigma$).

Finally, a scintillation counter V was placed at the third focus, or veto plane, of the beam. The size⁸ of this rectangular counter varied with the incident beam momentum and was chosen such that V vetoed unscattered beam tracks and scatterers corresponding to $-t < 0.001$ (GeV/c)².

III. DATA ACQUISITION

The data-collection logic consisted of a two-level trigger. The first level used the various scintillation counters of the apparatus; the second, an analog device called the hardware focus scatter detector (HFSD).¹¹ An event satisfying both levels is referred to as a SCATTER. As the

data-acquisition system is described in detail in Refs. 8 and 9, the system will be only briefly described here.

The basic criteria to pass the first level of the SCATTER trigger were

- (1) Reasonable incoming beam trajectory defined as $B1 \cdot B2 \cdot \overline{VH1}$ along with other beam-defining counters, not shown in Fig. 1, located upstream of the concrete block,
- (2) proper particle identification by the Čerenkov counters,
- (3) no other incident particle detected within ± 400 nsec of the trigger,
- (4) the particle traversed the entire apparatus, and
- (5) no signal from the veto V at the third focus.

A second level of triggering was necessary since the first level was dominated by beam halo. The HFSD provided the second level to the SCATTER trigger. This analog device performed two tests using the track coordinates as measured in the high-resolution PWC's. Acting as a hardware focus detector (HFD), the processor determined whether the track, as extrapolated from the coordinates measured in the two high resolution PWC's upstream of the target, intercepted a preset beam window in the veto plane. To pass the HFD test the track had to intercept the window in

TABLE I. Nuclear-target parameters.

Target	Z	A (amu)	Diameter (cm)	Length (cm)	Density (g/cm^3)	Radiation length, L_R (g/cm^2)	L/L_R
Be	4	9.01	5.40	1.600	1.85	65.19	0.045
C	6	12.01	5.73	1.259	1.64	42.70	0.048
Al	18	26.98	6.02	0.401	2.73	24.01	0.046
Cu	29	63.55	6.32	0.080	8.96	12.86	0.056
Sn	50	118.69	6.32	0.084	7.31	8.82	0.070
Pb	82	207.19	6.63	0.026	11.35	6.37	0.046

TABLE II. Cuts to extract elastic signal. Be; 175 GeV/c.

Cut	Fraction of events remaining after cut		
	π^+	K^+	p
(1) Track-reconstruction requirements on PWC coordinates.	0.741	0.741	0.741
(2) HFD test passed.	0.734	0.736	0.736
(3) Muon detector does not signal presence of a muon.	0.658	0.614	0.695
(4) No count from <i>VH2</i> and <i>VH3</i> .	0.626	0.585	0.657
(5) Outgoing particle trajectory traversed the area inside spectrometer magnet apertures.	0.623	0.583	0.654
(6) $[7.9]^2 \leq \text{recoil mass squared} \leq [8.8 \text{ GeV}/c^2]^2$.	0.596	0.554	0.624
(7) HSD test passed.	0.575	0.532	0.607
(8) Scatter vertex in target region.	0.292	0.258	0.363
(9) Outgoing particle trajectory passed ≥ 0.5 mm from edges of <i>V</i> .	0.282	0.249	0.354
(10) Track ≤ 1.5 cm from center of PWC station 4.	0.281	0.248	0.353
(11) Events whose trajectories were in region of $>90\%$ efficiency in PWC station 4.	0.280	0.247	0.351

both the x and y projections. The second requirement was that the data from the two upstream and the most downstream high-resolution chambers did not represent a collinear track. This test, with the processor in the hardware-scatter-detector (HSD) mode, was required in only one projection. The analog processor took about 5 μ sec to make its decision.

There were two additional trigger types recorded along with the scattered events; in both, the HFSD requirement was not necessary. One was a specified fraction of SCATTER triggers without the HFSD requirement used to study the HFSD performance and any biases it may have introduced into the data. No such biases were found. The second, BEAM, was a sample of incident beam particles used to provide information for alignment and absolute normalization.

The online computer, a PDP15/40,¹² recorded

approximately 500 triggers per one-second spill. Typically 400 were SCATTER's; the rest were the other trigger types. The relative fraction of events recorded involving a particular projectile type was scaled to result in an apparatus live time of 60%.

IV. DATA REDUCTION

We used the quantity q in the analysis where

$$q = \sqrt{-t} \simeq P_b \theta, \quad (1a)$$

where

$$P_b = \text{incident beam momentum,}$$

$$\theta = \text{scattering angle,}$$

and

$$d\sigma/dq = 2\sqrt{-t} d\sigma/dt. \quad (1b)$$

TABLE III. Cuts to extract elastic signal. Pb; 175 GeV/c.

Cut	Fraction of events remaining after cut		
	π^+	K^+	p
(1) Track-reconstruction requirements on PWC coordinates.	0.721	0.721	0.721
(2) HFD test passed.	0.708	0.718	0.715
(3) Muon detector does not signal presence of a muon.	0.636	0.592	0.680
(4) No count from <i>VH2</i> and <i>VH3</i> .	0.631	0.587	0.673
(5) Outgoing particle trajectory traversed the area inside of spectrometer magnet apertures.	0.630	0.587	0.673
(6) $[192.6]^2 \leq \text{recoil mass squared} \leq [193.4 \text{ (GeV}/c^2)]^2$.	0.601	0.556	0.638
(7) HSD test passed.	0.571	0.527	0.608
(8) Scatter vertex in target region.	0.181	0.172	0.182
(9) Outgoing particle trajectory passed ≥ 0.5 mm from edges of <i>V</i> .	0.170	0.162	0.171
(10) Track ≤ 1.5 cm from center of PWC station 4.	0.170	0.162	0.171
(11) Events whose trajectories were in region of $>90\%$ efficiency in PWC station 4.	0.170	0.162	0.171

TABLE IV. Hadron-nucleus elastic-scattering event totals (in thousands) for $-t > -t_{\min}$.

Momentum (GeV/c)	Target	π^+	K^+	p^+	π^-	K^-	\bar{p}
175 [$t_{\min} = -0.0018$ (GeV/c) ²]	Be	16.4	7.6	38.0	11.8	4.5	1.5
	C	18.5	9.0	41.2	9.2	3.4	1.1
	Al	12.0	6.0	23.8	5.1	1.9	0.5
	Cu	8.9	4.5	14.9	6.8	2.7	0.6
	Sn	12.6	6.9	18.9	8.8	3.6	0.7
	Pb	12.3	7.0	17.1	8.8	3.9	0.7
125 [$t_{\min} = -0.0016$ (GeV/c) ²]	Be	9.4	3.7	23.3			
	Al	11.5	6.6	23.3			
	Pb	9.6	6.9	14.0			
70 [$t_{\min} = -0.0013$ (GeV/c) ²]	Be	8.2	4.1	13.7	10.0	4.4	8.1
	C	7.3	3.8	11.7	8.8	4.3	6.7
	Al	11.5	6.1	15.0	13.8	13.7	19.1
	Cu	11.0	6.4	11.0	8.2	8.4	9.2
	Sn	15.8	9.5	16.2	15.5	16.6	15.6
	Pb	9.8	6.1	8.9	7.1	7.6	6.4

There were two reasons for this choice. The first was that the resolution of the apparatus was constant in θ (30 μ rad; σ). The second reason was that $d\sigma/dq$ vs q is a more slowly varying function than $d\sigma/dt$ vs t . Thus the binning of $d\sigma/dq$ in equal q bins populates the bins more uniformly. This reduced the sensitivity of the fitting procedure to the following effects: (1) Integration of the cross section over the bin, and (2) the migration of events from bin to bin due to resolution.

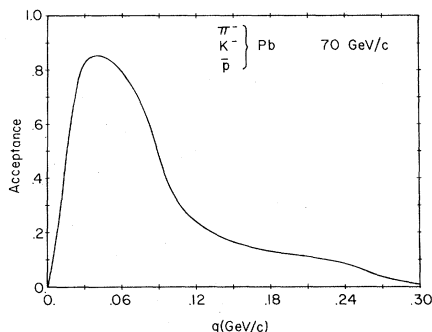
The data-reduction process kept only those events with unambiguous single tracks before and after the nuclear target. The major cuts applied to extract the elastic signal are given for some specific cases in Tables II and III. The number of events after cuts is presented in Table IV. The two cuts which eliminated the greatest fraction of triggers were the track reconstruction requirements on the PWC coordinates and that the scatter vertex was in the target region. The cut on

the scatter-vertex position eliminated a large fraction of events because the trigger accepted scatters originating from the high-resolution PWC's immediately upstream and downstream of the target.

Next the target-full and -empty q distributions were normalized, and then a target-empty subtraction was performed. The normalization was calculated using those BEAM events that traversed the entire apparatus; thus there was no need to make any correction for the absorption of scattered particles downstream of the target or for overall PWC inefficiencies. The target-empty subtraction is q dependent and increases with increasing projectile momentum. The correction is largest for the heaviest target. It is less than

TABLE V. Incoherent-scattering-term parameters and nuclear charge radius R .

Reaction	Momentum (GeV/c)	N_A	σ_{hp}^a (mb)	b [(GeV/c) ⁻²]	R (fm)
π^\pm, K^\pm -Be	175, 125, 70	3.5	25, 20	10	2.20
p, \bar{p} -Be	175, 125, 70	3.5	40	12	2.20
π^\pm, K^\pm -C	175, 70	3.4	25, 20	10	2.42
p, \bar{p} -C	175, 70	3.4	40	12	2.42
π^\pm, K^\pm -Al	175, 125, 70	4.5	25, 20	10	3.02
p, \bar{p} -Al	175, 125, 70	4.5	40	12	3.02
π^\pm, K^\pm -Cu	175, 70	6.7	25, 20	10	3.66
p, \bar{p} -Cu	175, 70	6.7	40	12	3.66
π^\pm, K^\pm -Sn	175, 70	8.2	25, 20	10	4.55
p, \bar{p} -Sn	175, 70	8.2	40	12	4.55
π^\pm, K^\pm -Pb	175, 125, 70	9.5	25, 20	10	5.42
p, \bar{p} -Pb	175, 125, 70	9.5	40	12	5.42

^a Second entry refers to the kaon case.FIG. 2. Apparatus acceptance for π^+ , K^+ , and \bar{p} scattering from Pb at incident momentum of 70 GeV/c.

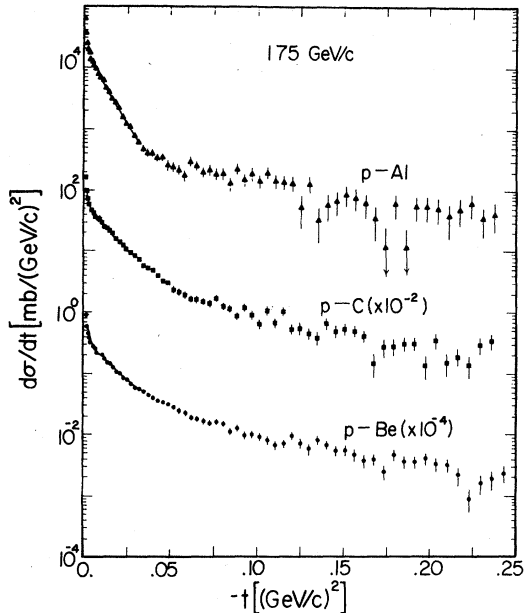


FIG. 3. $d\sigma/dt$ for elastic scattering at incident beam momentum of 175 GeV/c for the following: p -Be, p -C, p -Al; solid lines present results of a fit of the data to Eq. (4) (see text and footnote 18).

1.5% in all q bins for the Pb target at 70 GeV/c; at 175 GeV/c it is approximately 13 and 9%, respectively, for Pb and Be in the smallest q bin.

To extract the physics parameters of interest,

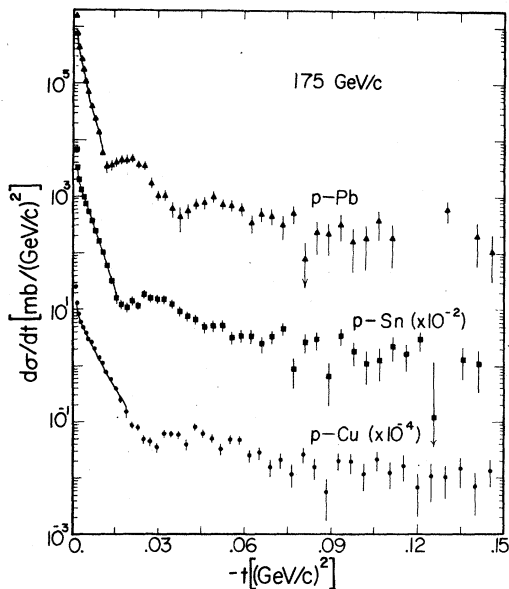


FIG. 4. $d\sigma/dt$ for elastic scattering at incident beam momentum of 175 GeV/c for the following: p -Cu, p -Sn, p -Pb; solid lines present results of a fit of the data to Eq. (4) (see text and footnote 18).

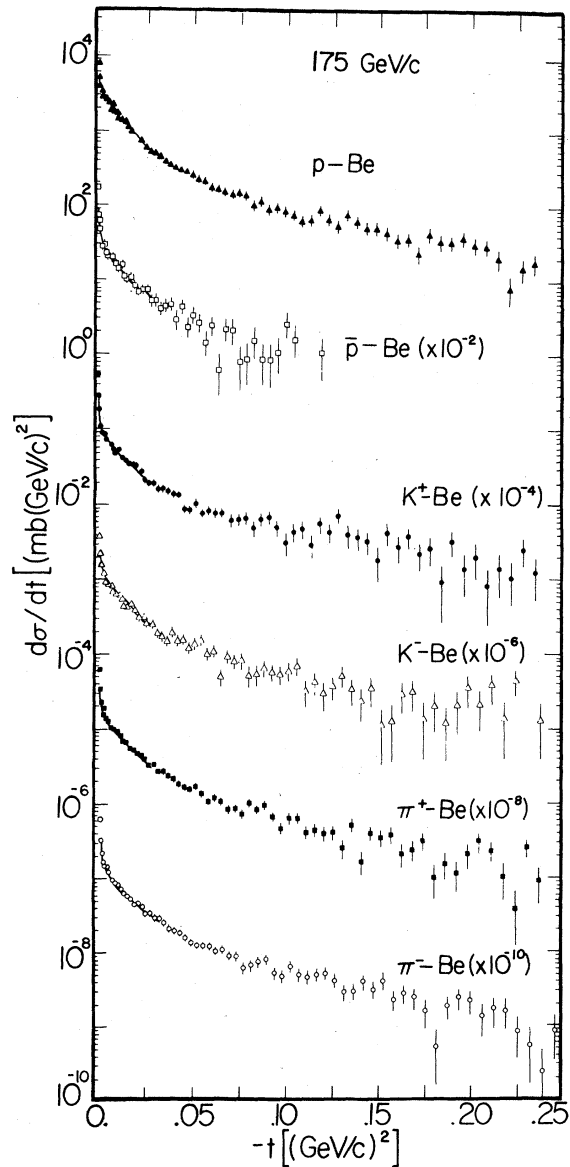


FIG. 5. $d\sigma/dt$ for elastic scattering at incident beam momentum of 175 GeV/c for the following: p -Be, \bar{p} -Be, K^+ -Be, K^- -Be, π^+ -Be, π^- -Be; solid lines present results of a fit of the data to Eq. (4) (see text and footnote 18).

a theoretical form of $d\sigma/dq$ was corrected for the apparatus acceptance and then compared to the data. A Monte Carlo program calculated the acceptance as a function of q . Events were generated with the scattering vertex in the nuclear target with a flat distribution in q and then were traced through the apparatus. The incident-beam phase space was provided by the beam tracks. Multiple scattering of the particle was simulated at the appropriate places and account was taken of any

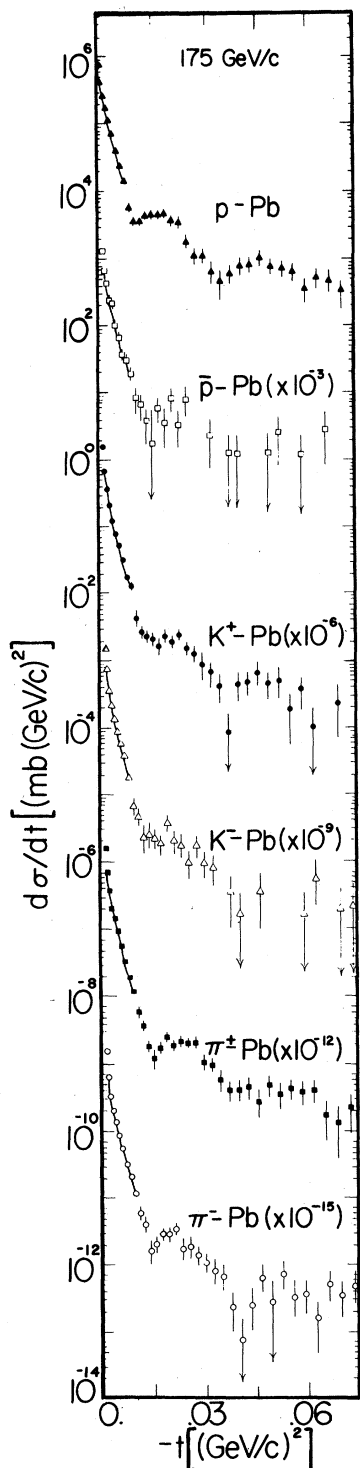


FIG. 6. $d\sigma/dt$ for elastic scattering at incident beam momentum of 175 GeV/c for the following: p -Pb, \bar{p} -Pb, K^+ -Pb, K^- -Pb, π^+ -Pb, π^- -Pb; solid lines present results of a fit of the data to Eq. (4) (see text and footnote 18).

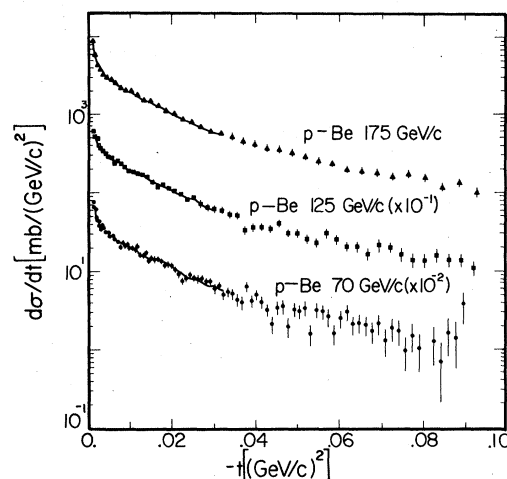


FIG. 7. $d\sigma/dt$ for p -Be elastic scattering at the following incident momenta: 175, 125, 70 GeV/c; solid lines present results of a fit of the data to Eq. (4) (see text and footnote 18).

local PWC inefficiencies and of effects of the finite resolution. The acceptance was found to be projectile independent and is shown in Fig. 2 for one particular case.

To fit the data, we used a least-squares minimization procedure which employed the program MINUIT.¹³ A theoretical cross section $d\sigma/dq$ (see Sec. V) was convoluted with the acceptance. This convolution took into account migration of events from one data bin to another. Next the convoluted theoretical form was compared to the quantity

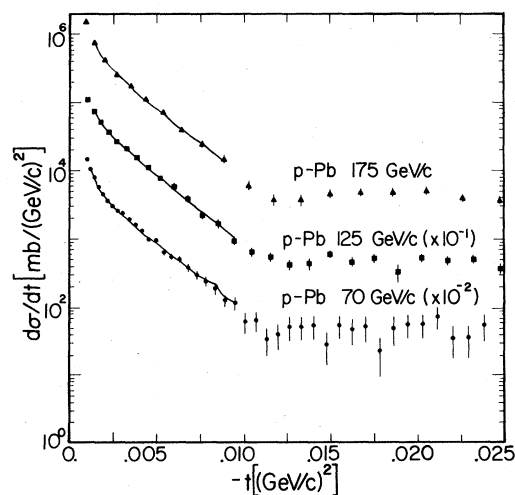


FIG. 8. $d\sigma/dt$ for p -Pb elastic scattering at the following incident momenta: 175, 125, 70 GeV/c; solid lines present results of a fit of the data to Eq. (4) (see text and footnote 18).

TABLE VI. Values of N_0 (overall normalization), b_A (forward slope for hadron-nucleus coherent scattering), and N_N (normalization for hadron-nucleus scattering) as obtained from the fits. Systematic errors are in parentheses. There is an additional uncertainty on b_A of $\pm 4\%$ for Be, $\pm 3\%$ for C, $\pm 2\%$ for Al, $\pm 1\%$ for Cu, $\pm 0.5\%$ for Sn, and $\pm 0.25\%$ for Pb, which is due to uncertainty in the values used in the parametrization of the incoherent scattering term in Eq. (4) (see text).

	$ t $ Range [(GeV/c) ²]	N_0	N_N (mb)		b_A [(GeV/c) ⁻²]	χ^2/DOF
175 GeV/c: π^+, K^+, p						
π^+ -Be	0.0018-0.0330	$0.86 \pm 0.05(0.04)$	$182.2 \pm 7.2(10.0)$	[-13.2] ^a	$64.9 \pm 1.5(3.0)$	18.0/18
K^+ -Be	0.0018-0.0330	$0.86 \pm 0.05(0.06)$	$149.3 \pm 7.4(8.0)$	[-10.8]	$58.0 \pm 2.2(2.0)$	20.1/18
p -Be	0.0018-0.0330	$1.08 \pm 0.06(0.05)$	$249.2 \pm 8.3(10.0)$	[9.8]	$74.7 \pm 1.0(1.5)$	20.3/18
π^+ -C	0.0018-0.0330	$0.82 \pm 0.04(0.04)$	$244.9 \pm 7.5(12.0)$	[-23.1]	$67.6 \pm 1.3(3.0)$	21.0/18
K^+ -C	0.0018-0.0330	$0.87 \pm 0.04(0.03)$	$195.4 \pm 7.5(5.0)$	[-13.1]	$60.4 \pm 2.0(2.0)$	18.3/18
p -C	0.0018-0.0330	$0.91 \pm 0.04(0.03)$	$345.2 \pm 9.9(15.0)$	[-15.9]	$74.0 \pm 1.0(3.0)$	21.6/18
π^+ -Al	0.0018-0.0330	$0.76 \pm 0.04(0.05)$	$507.8 \pm 16.9(15.0)$	[-25.1]	$106.9 \pm 2.0(2.0)$	22.1/18
K^+ -Al	0.0018-0.0330	$0.80 \pm 0.04(0.02)$	$442.1 \pm 19.4(10.0)$	[-46.7]	$108.6 \pm 3.0(2.0)$	22.5/18
p -Al	0.0018-0.0330	$0.72 \pm 0.04(0.03)$	$764.3 \pm 23.5(15.0)$	[-115.8]	$120.3 \pm 1.5(2.0)$	21.9/18
π^+ -Cu	0.0018-0.0195	$0.73 \pm 0.03(0.04)$	$1117.4 \pm 47.9(40.0)$	[-162.8]	$190.3 \pm 4.8(3.0)$	13.4/12
K^+ -Cu	0.0018-0.0195	$0.73 \pm 0.04(0.06)$	$926.1 \pm 54.0(45.0)$	[-134.8]	$185.3 \pm 7.4(3.0)$	9.5/12
p -Cu	0.0018-0.0195	$0.54 \pm 0.03(0.05)$	$1835.0 \pm 79.9(60.0)$	[-486.6]	$217.8 \pm 3.2(2.0)$	14.2/12
π^+ -Sn	0.0018-0.0160	$0.62 \pm 0.03(0.04)$	$2320.3 \pm 102.0(80.0)$	[-493.2]	$312.9 \pm 6.2(3.0)$	11.7/10
K^+ -Sn	0.0018-0.0160	$0.69 \pm 0.03(0.03)$	$1933.9 \pm 106.4(50.0)$	[-327.5]	$309.8 \pm 8.7(3.0)$	12.8/10
p -Sn	0.0018-0.0160	$0.47 \pm 0.03(0.05)$	$3465.6 \pm 157.6(130.0)$	[-1089.9]	$338.3 \pm 4.6(3.0)$	13.1/10
π^+ -Pb	0.0018-0.0096	$0.61 \pm 0.04(0.03)$	$3818.4 \pm 279.3(150.0)$	[-836.0]	$436.7 \pm 15.5(8.0)$	7.8/ 6
K^+ -Pb	0.0018-0.0096	$0.67 \pm 0.04(0.05)$	$3210.1 \pm 286.7(130.0)$	[-582.5]	$410.5 \pm 20.9(7.0)$	6.1/ 6
p -Pb	0.0018-0.0096	$0.55 \pm 0.03(0.05)$	$4803.3 \pm 219.6(80.0)$	[-1241.0]	$455.3 \pm 10.1(5.0)$	6.5/ 6
125 GeV/c: π^+, K^+, p						
π^+ -Be	0.0016-0.0306	$0.80 \pm 0.06(0.05)$	$190.3 \pm 9.7(6.0)$	[-20.11] ^a	$65.6 \pm 2.1(1.0)$	24.2/25
K^+ -Be	0.0016-0.0306	$0.88 \pm 0.06(0.03)$	$145.9 \pm 8.1(3.0)$	[-9.01]	$60.1 \pm 2.4(1.0)$	23.1/25
p -Be	0.0016-0.0306	$0.93 \pm 0.07(0.04)$	$269.0 \pm 12.4(8.0)$	[-9.6]	$70.7 \pm 1.3(0.7)$	27.4/25
π^+ -Al	0.0016-0.0306	$0.77 \pm 0.04(0.02)$	$521.4 \pm 17.4(11.0)$	[-63.9]	$108.1 \pm 2.2(1.7)$	27.2/25
K^+ -Al	0.0016-0.0306	$0.76 \pm 0.04(0.03)$	$442.0 \pm 19.2(15.0)$	[-56.7]	$102.5 \pm 3.2(2.9)$	26.0/25
p -Al	0.0016-0.0306	$0.70 \pm 0.04(0.02)$	$780.8 \pm 25.9(14.0)$	[-127.6]	$119.1 \pm 1.5(1.8)$	26.5/25
π^+ -Pb	0.0016-0.0100	$0.50 \pm 0.04(0.03)$	$4599.0 \pm 349.3(150.0)$	[-1347.0]	$448.1 \pm 13.6(4.0)$	4.8/10
K^+ -Pb	0.0016-0.0100	$0.59 \pm 0.04(0.03)$	$3864.7 \pm 319.5(175.0)$	[-896.1]	$436.2 \pm 16.6(6.0)$	9.7/10
p -Pb	0.0016-0.0100	$0.41 \pm 0.04(0.04)$	$6219.2 \pm 461.0(180.0)$	[-2237.0]	$475.3 \pm 10.5(4.0)$	11.0/10
70 GeV/c: π^+, K^+, p						
π^+ -Be	0.0013-0.0324	$1.00 \pm 0.05(0.04)$	$170.9 \pm 6.7(4.0)$	[0.0] ^a	$65.1 \pm 2.8(2.0)$	32.2/45
K^+ -Be	0.0013-0.0324	$1.02 \pm 0.06(0.03)$	$135.8 \pm 6.9(5.0)$	[1.4]	$61.8 \pm 4.4(6.0)$	52.1/45
p -Be	0.0013-0.0324	$1.06 \pm 0.07(0.02)$	$251.6 \pm 10.8(7.0)$	[7.4]	$70.7 \pm 4.8(3.0)$	47.2/45
π^+ -C	0.0013-0.0324	$0.86 \pm 0.04(0.02)$	$237.8 \pm 9.0(6.0)$	[-17.3]	$63.5 \pm 2.8(2.0)$	44.1/45
K^+ -C	0.0013-0.0324	$1.06 \pm 0.05(0.02)$	$167.6 \pm 7.7(7.0)$	[5.0]	$58.7 \pm 4.3(5.0)$	46.6/45
p -C	0.0013-0.0324	$1.00 \pm 0.04(0.03)$	$325.3 \pm 7.5(7.0)$	[0.0]	$70.5 \pm 2.4(2.0)$	46.4/45
π^+ -Al	0.0013-0.0324	$0.85 \pm 0.03(0.04)$	$487.6 \pm 13.8(10.0)$	[-38.1]	$107.0 \pm 3.0(2.0)$	33.8/45
K^+ -Al	0.0013-0.0324	$0.87 \pm 0.03(0.02)$	$408.9 \pm 15.5(8.0)$	[-27.5]	$105.7 \pm 4.4(2.0)$	45.6/45
p -Al	0.0013-0.0324	$0.82 \pm 0.04(0.03)$	$720.3 \pm 22.6(7.0)$	[-68.0]	$118.8 \pm 2.4(3.0)$	50.7/45
π^+ -Cu	0.0013-0.0144	$0.77 \pm 0.03(0.02)$	$1090.6 \pm 42.9(15.0)$	[-133.6]	$187.4 \pm 6.9(2.0)$	26.8/27
K^+ -Cu	0.0013-0.0144	$0.79 \pm 0.03(0.02)$	$901.1 \pm 47.6(15.0)$	[-100.2]	$173.6 \pm 10.1(2.0)$	25.9/27
p -Cu	0.0013-0.0144	$0.70 \pm 0.03(0.02)$	$1477.5 \pm 59.1(12.0)$	[-241.3]	$184.0 \pm 5.6(2.0)$	28.2/27
π^+ -Sn	0.0013-0.0110	$0.73 \pm 0.02(0.02)$	$1905.2 \pm 76.3(55.0)$	[-277.4]	$259.4 \pm 9.5(3.0)$	14.1/22
K^+ -Sn	0.0013-0.0110	$0.79 \pm 0.03(0.02)$	$1512.2 \pm 83.2(36.0)$	[-168.1]	$229.8 \pm 13.9(4.0)$	14.3/22
p -Sn	0.0013-0.0110	$0.65 \pm 0.03(0.02)$	$2544.3 \pm 107.1(30.0)$	[-493.0]	$283.5 \pm 8.3(2.0)$	26.8/22
π^+ -Pb	0.0013-0.0110	$0.65 \pm 0.03(0.01)$	$3795.5 \pm 220.1(20.0)$	[-735.5]	$421.3 \pm 13.0(5.0)$	21.6/22
K^+ -Pb	0.0013-0.0110	$0.75 \pm 0.04(0.02)$	$3028.9 \pm 231.9(50.0)$	[-405.8]	$401.3 \pm 19.7(8.0)$	24.4/22
p -Pb	0.0013-0.0110	$0.62 \pm 0.04(0.01)$	$4348.2 \pm 273.0(45.0)$	[-924.4]	$431.8 \pm 13.2(5.0)$	23.8/22

TABLE VI. (Continued.)

	$ t $ Range [(GeV/c) ²]	N_0	N_N (mb)		b_A [(GeV/c) ⁻²]	χ^2/DOF
70 GeV/c: π^-, K^-, \bar{p}						
π^- -Be	0.0013-0.0324	0.95±0.04(0.02)	165.9±	5.8(2.0)	[-4.2] ^a	61.0± 2.5(1.5) 45.9/46
K^- -Be	0.0013-0.0324	0.92±0.05(0.05)	150.7±	7.6(10.0)	[-6.2]	69.7± 4.0(7.0) 47.2/46
\bar{p} -Be	0.0013-0.0324	0.90±0.09(0.06)	289.5±	17.6(10.0)	[-14.9]	68.5± 3.6(4.0) 46.4/46
π^- -C	0.0013-0.0324	0.88±0.03(0.02)	222.3±	7.4(4.0)	[-13.8]	58.6± 2.6(3.0) 45.8/45
K^- -C	0.0013-0.0324	0.93±0.05(0.03)	207.6±	9.5(5.0)	[-7.4]	68.2± 4.1(3.0) 51.7/45
\bar{p} -C	0.0013-0.0324	0.82±0.08(0.04)	391.7±	23.1(8.0)	[-37.0]	72.3± 2.6(4.0) 50.6/45
π^- -Al	0.0013-0.0324	0.79±0.02(0.02)	483.9±	12.4(5.0)	[-53.8]	103.8± 2.7(1.5) 37.8/45
K^- -Al	0.0013-0.0324	0.84±0.02(0.03)	428.8±	11.4(6.0)	[-35.7]	103.3± 3.1(3.0) 49.2/45
\bar{p} -Al	0.0013-0.0324	0.63±0.03(0.04)	868.8±	28.7(11.0)	[-179.2]	121.7± 2.0(2.0) 53.8/45
π^- -Cu	0.0013-0.0144	0.69±0.03(0.03)	1077.5±	48.8(55.0)	[-182.5]	172.4± 7.7(3.0) 29.2/27
K^- -Cu	0.0013-0.0144	0.77±0.03(0.03)	900.4±	40.6(55.0)	[-110.3]	162.1± 8.5(4.0) 16.4/27
\bar{p} -Cu	0.0013-0.0144	0.56±0.04(0.03)	1755.5±	90.9(75.0)	[-441.8]	199.3± 6.4(3.0) 26.3/27
π^- -Sn	0.0013-0.0110	0.67±0.02(0.02)	1825.6±	73.5(40.0)	[-331.8]	253.9± 9.4(3.0) 21.7/22
K^- -Sn	0.0013-0.0110	0.78±0.02(0.02)	1524.8±	62.2(25.0)	[-178.1]	237.8± 9.9(3.0) 24.3/22
\bar{p} -Sn	0.0013-0.0110	0.61±0.03(0.02)	2649.1±	113.1(90.0)	[-580.1]	282.0± 8.0(3.0) 24.1/22
π^- -Pb	0.0013-0.0110	0.65±0.03(0.03)	3186.6±	213.8(40.0)	[-617.5]	386.6±16.4(4.0) 17.1/22
K^- -Pb	0.0013-0.0110	0.67±0.03(0.05)	3088.6±	194.3(60.0)	[-560.5]	386.4±15.5(5.0) 23.7/22
\bar{p} -Pb	0.0013-0.0110	0.44±0.04(0.03)	5616.4±	408.7(150.0)	[-1890.9]	461.6±13.7(10.0) 25.2/22
175 GeV/c: π^-, K^-, \bar{p}						
π^- -Be	0.0018-0.0333	0.96±0.06(0.06)	168.4±	7.4(7.0)	[-3.4] ^a	65.8± 1.8(4.0) 20.9/18
K^- -Be	0.0018-0.0333	1.21±0.09(0.05)	128.0±	7.5(5.0)	[12.8]	61.6± 3.1(2.0) 11.1/18
\bar{p} -Be	0.0018-0.0333	1.64±0.31(0.20)	191.0±	25.1(16.0)	[53.6]	79.0± 6.4(4.0) 7.6/18
π^- -C	0.0018-0.0333	0.86±0.05(0.06)	237.1±	10.3(7.0)	[-17.2]	67.5± 1.9(2.0) 20.3/18
K^- -C	0.0018-0.0333	1.05±0.08(0.06)	184.8±	11.3(7.0)	[4.6]	68.0± 3.6(2.5) 20.1/18
\bar{p} -C	0.0018-0.0333	1.12±0.26(0.08)	317.6±	48.2(15.0)	[18.5]	79.6± 5.6(2.0) 21.2/18
π^- -Al	0.0018-0.0333	0.83±0.05(0.06)	477.7±	23.4(18.0)	[-42.5]	106.2± 3.2(4.0) 19.5/18
K^- -Al	0.0018-0.0333	0.96±0.08(0.05)	378.7±	26.8(10.0)	[-7.7]	94.3± 5.2(3.0) 9.4/18
\bar{p} -Al	0.0018-0.0333	0.15±0.04(0.10)	1820.9±	39.6(60.0)	[-1115.7]	137.8± 4.3(4.0) 24.8/18
π^- -Cu	0.0018-0.0200	0.63±0.04(0.05)	1208.9±	61.8(45.0)	[-249.4]	193.4± 5.3(2.0) 10.6/12
K^- -Cu	0.0018-0.0200	0.75±0.05(0.06)	978.7±	72.3(40.0)	[-131.1]	193.8± 9.9(3.0) 12.0/12
\bar{p} -Cu	0.0018-0.0200	0.47±0.19(0.06)	2035.5±	507.4(100.0)	[-640.0]	225.9±15.3(5.0) 13.0/12
π^- -Sn	0.0018-0.0160	0.55±0.03(0.02)	2310.8±	123.6(70.0)	[-597.1]	299.1± 7.6(3.0) 10.6/10
K^- -Sn	0.0018-0.0160	0.60±0.05(0.04)	2057.4±	163.9(120.0)	[-463.7]	294.4±12.5(3.0) 9.7/10
\bar{p} -Sn	0.0018-0.0160	0.31±0.11(0.08)	4469.9±	939.9(100.0)	[-1981.2]	348.9±20.8(8.0) 12.3/10
π^- -Pb	0.0018-0.0100	0.59±0.04(0.06)	3594.9±	284.8(175.0)	[-833.6]	406.5±17.1(9.0) 5.6/ 6
K^- -Pb	0.0018-0.0100	0.70±0.06(0.06)	3246.5±	365.6(280.0)	[-530.2]	418.6±25.9(18.0) 11.2/ 6
\bar{p} -Pb	0.0018-0.0100	0.46±0.17(0.13)	5271.5±	1772.6(400.0)	[-1696.2]	434.9±54.1(20.0) 6.8/ 6

^a The numbers in square brackets represent the uncertainty in N_N due to the deviation of N_0 from unity. These uncertainties are not symmetric and are given by $[(1-N_0)/|1-N_0|](1-\sqrt{N_0})N_N$. The uncertainty in the other direction is 0.0. If N_0 is less (greater) than 1.0, then this uncertainty increases only the lower (upper) limit on N_N .

$\delta(q)$, where

$$\delta(q) = \frac{1}{\Delta \cdot \Gamma} \left[\frac{N_s^F(q)}{I_0^F} - \frac{N_s^E(q)}{I_0^E} \right], \quad (2)$$

where

$N_s^F(q), N_s^E(q)$ = number of scattered particles in each q bin that pass all cuts for target full, target empty,

I_0^F, I_0^E = number of incident-beam particles for target full, target empty,

$\Delta = q$ bin size,

$\Gamma = N\rho x/A$,
 N = Avogadro's number,
 ρ = target density,
 x = target length,
 A = atomic weight.

The $d\sigma/dt$ distribution was calculated [using Eq. (1b)]

$$d\sigma/dt = \delta(q)/[2q\epsilon(q)], \quad (3)$$

where

$\epsilon(q)$ = acceptance as a function of q .

V. RESULTS

We parametrize the theoretical cross section as

$$\left(\frac{d\sigma}{dq}\right)_{\text{th}} = N_0 \left(\frac{2q}{\Gamma w^2} \exp(-q^2/w^2) + \frac{8\pi e^4 Z^2}{q^3} G_P^2 G_T^2 \left\{ 1 - \frac{4w^2}{q^2} \left[1 + \frac{2}{\beta} \ln\left(\frac{2q}{5w}\right) \right] \right\}^{-1} + \frac{q N_N^2}{8\pi \hbar^2} \exp(-b_A q^2) + \frac{N_A q \sigma_{hp}^2}{8\pi \hbar^2} \exp(b_p q^2) \right), \quad (4)$$

where the Coulomb-nuclear interference term is neglected, and

N_0 = normalization factor,

β, w = multiple-Coulomb-scattering parameters,¹⁴

Z = atomic number,

G_P = electromagnetic form factor of projectile,¹⁵

G_T = electromagnetic form factor of nuclear target,¹⁵

N_N = normalization for projectile-nucleus scattering,

b_A = forward slope for coherent projectile-nucleus elastic scattering,

N_A = number of individual nucleons involved in incoherent projectile-nucleus scattering,

σ_{hp} = projectile-proton total cross section,

b_p = forward slope of projectile-proton elastic scattering,

Γ = as defined in Eq. (2).

The terms in Eq. (4) represent the following processes. The first term represents multiple Coulomb scattering and the second term represents single Coulomb scattering. The correction factor to the second term, in braces, takes into account the effects of plural Coulomb scattering.^{14,16} The third term describes coherent elastic scattering (from the nucleus as a whole); the fourth describes incoherent scattering (from individual nucleons). The incoherent scattering term represents interactions which excite or break up the nucleus (true elastic scattering leaves the nucleus in its ground state) but which are included in the elastic signal due to the apparatus' momentum resolution. The parametrization of the incoherent scattering follows the approach of Ref. 3. The parameters for the incoherent-scattering term were taken from Ref. 3 and are given in Table V. The fitting program fits for N_0 , b_A , and N_N only.

Tables of $d\sigma/dt$ for the reactions studied are given in Ref. 17. Figures 3–8 present $d\sigma/dt$ distributions for some of the reactions measured. Figures 3 and 4 show $d\sigma/dt$ distributions for proton scattering from the various targets (Be, C, Al, Cu, Sn, and Pb) at an incident momentum of

175 GeV/c. Figures 5 and 6 present the scattering from Be and Pb targets, respectively, of the various incident projectiles (π^\pm , K^\pm , p , and \bar{p}) at an incident momentum of 175 GeV/c. Finally, Figs. 7 and 8 present the momentum dependence (incident momenta of 70, 125, and 175 GeV/c) of $d\sigma/dt$ for proton scattering from Be and Pb targets, respectively.

We note that as the atomic number of the target increases, the $d\sigma/dt$ distributions become more sharply peaked. For the Cu, Sn, and Pb target data, a secondary maximum is observed. The position in t of the second maximum decreases as the atomic number of the target increases. The shape of the t distributions does not depend in any significant manner on the incident beam momentum.

Table VI presents values of N_0 , b_A , and N_N as derived from the fits. The solid lines in Figs. 3–8 present the results of these fits [using the parametrization of Eq. (4)]. Figure 9 shows the relative contribution of each term of Eq. (4) for two representative cases.

The systematic errors were calculated in the following manner. A series of fits were performed varying the cut on a particular kinematic variable (for example recoil mass squared) while keeping

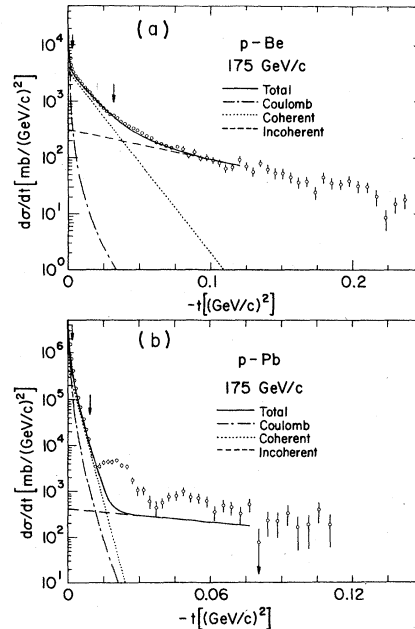


FIG. 9. Contributions of various terms in Eq. (4) (see text) to (a) p -Be at 175 GeV/c (b) p -Pb at 175 GeV/c. Dotted-dashed line is the contribution of Coulomb scattering. Dotted line is the contribution of coherent scattering. Dashed line is the contribution of incoherent scattering. Solid line is the sum of all contributions. Arrows indicate region of t fit over.

TABLE VII. Values of forward slope for hadron-nucleus coherent scattering, b_A , of $d\sigma/dt$ in the region of $0.0018 \leq -t \leq 0.0100$ (GeV/c)².

	Momentum (GeV/c)	b_A [(GeV/c) ⁻²]	χ^2/DOF		Momentum (GeV/c)	b_A [(GeV/c) ⁻²]	χ^2/DOF
π^+ -Be	175	64.4 ± 2.7	2.3/ 8	p -Al	125	117.7 ± 2.7	13.7/12
K^+ -Be	175	57.2 ± 4.1	11.7/ 8	π^+ -Pb	125	449.4 ± 13.3	5.5/12
p -Be	175	77.8 ± 2.5	9.1/ 8	K^+ -Pb	125	435.3 ± 16.4	10.3/12
π^- -Be	175	63.3 ± 3.5	6.8/ 8	p -Pb	125	475.9 ± 10.1	12.7/12
K^- -Be	175	60.9 ± 5.6	3.7/ 8	π^+ -Be	70	65.0 ± 3.5	8.7/21
\bar{p} -Be	175	75.4 ± 9.7	3.9/ 8	K^+ -Be	70	60.9 ± 5.3	22.1/21
π^+ -C	175	62.3 ± 3.3	10.6/ 8	p -Be	70	71.9 ± 6.3	23.9/21
K^+ -C	175	57.5 ± 5.2	5.1/ 8	π^- -Be	70	60.3 ± 5.3	20.2/21
p -C	175	74.1 ± 2.7	10.2/ 8	K^- -Be	70	64.8 ± 7.3	24.9/21
π^- -C	175	65.4 ± 4.2	6.4/ 8	\bar{p} -Be	70	68.9 ± 6.5	19.6/21
K^- -C	175	59.8 ± 6.0	6.5/ 8	π^+ -C	70	61.1 ± 4.3	13.7/21
\bar{p} -C	175	85.5 ± 9.5	10.2/ 8	K^+ -C	70	58.6 ± 6.7	16.1/21
π^+ -Al	175	106.3 ± 4.8	12.2/ 8	p -C	70	70.9 ± 3.8	24.2/21
K^+ -Al	175	111.1 ± 5.2	10.3/ 8	π^- -C	70	57.4 ± 5.6	26.3/21
p -Al	175	121.9 ± 2.6	11.4/ 8	K^- -C	70	69.3 ± 6.6	24.0/21
π^- -Al	175	109.2 ± 7.3	9.6/ 8	\bar{p} -C	70	69.5 ± 3.5	25.6/21
K^- -Al	175	87.8 ± 9.4	6.5/ 8	π^+ -Al	70	107.6 ± 7.1	21.1/21
\bar{p} -Al	175	131.4 ± 10.7	10.9/ 8	K^+ -Al	70	107.4 ± 8.2	15.6/21
π^+ -Cu	175	186.9 ± 5.4	8.5/ 8	p -Al	70	117.0 ± 5.5	25.6/21
K^+ -Cu	175	183.6 ± 7.8	3.6/ 8	π^- -Al	70	105.0 ± 4.4	14.8/21
p -Cu	175	217.4 ± 4.3	11.5/ 8	K^- -Al	70	102.4 ± 4.5	19.5/21
π^- -Cu	175	192.8 ± 8.2	3.8/ 8	\bar{p} -Al	70	120.4 ± 3.8	21.0/21
K^- -Cu	175	192.7 ± 13.1	8.3/ 8	π^+ -Cu	70	185.9 ± 7.9	23.8/21
\bar{p} -Cu	175	218.2 ± 21.8	7.2/ 8	K^+ -Cu	70	171.8 ± 11.1	23.3/21
π^+ -Sn	175	308.1 ± 7.3	10.1/ 8	p -Cu	70	182.9 ± 6.3	25.7/21
K^+ -Sn	175	299.8 ± 11.2	10.5/ 8	π^- -Cu	70	167.1 ± 8.2	18.8/21
p -Sn	175	335.1 ± 5.3	12.1/ 8	K^- -Cu	70	159.9 ± 9.9	13.4/21
π^- -Sn	175	297.6 ± 7.9	4.1/ 8	\bar{p} -Cu	70	191.3 ± 9.5	15.8/21
K^- -Sn	175	293.8 ± 13.2	9.3/ 8	π^+ -Sn	70	259.4 ± 7.8	12.4/21
\bar{p} -Sn	175	345.5 ± 21.6	10.6/ 8	K^+ -Sn	70	229.2 ± 12.1	13.8/21
π^+ -Pb	175	435.2 ± 15.2	8.2/ 8	p -Sn	70	284.0 ± 7.4	25.1/21
K^+ -Pb	175	411.6 ± 20.1	6.7/ 8	π^- -Sn	70	252.6 ± 9.7	19.1/21
p -Pb	175	455.7 ± 9.8	7.2/ 8	K^- -Sn	70	237.1 ± 10.3	24.8/21
π^- -Pb	175	407.2 ± 16.8	6.2/ 8	\bar{p} -Sn	70	281.7 ± 8.5	26.4/21
K^- -Pb	175	419.3 ± 25.4	10.7/ 8	π^+ -Pb	70	420.8 ± 12.7	21.3/21
\bar{p} -Pb	175	433.9 ± 53.2	7.4/ 8	K^+ -Pb	70	403.4 ± 18.8	25.2/21
π^+ -Be	125	64.1 ± 3.9	15.7/12	p -Pb	70	430.2 ± 12.9	23.5/21
K^+ -Be	125	57.8 ± 5.2	10.6/12	π^- -Pb	70	384.4 ± 15.7	15.9/21
p -Be	125	71.5 ± 3.3	14.3/12	K^- -Pb	70	385.1 ± 15.3	22.3/21
π^- -Al	125	110.1 ± 4.4	9.3/12	\bar{p} -Pb	70	464.2 ± 13.2	24.8/21
K^+ -Al	125	98.2 ± 5.1	11.9/12				

all other cuts constant. The systematic error was then defined as the absolute value of the range the parameters of interest (i.e., N_0 , b_A , and N_N) varied for the series of fits. In addition, we investigated the dependence of the results on the values of N_A and b_p in the incoherent scattering term (see Table V). A variation of 30% in N_A leads to negligible change in N_0 and N_N , however, there is some effect on b_A . This effect on b_A is 4% for Be, 3% for C, 2% for Al, 1% for Cu, 0.5% for Sn, and 0.25% for Pb. A variation of one unit in b_p has

a negligible effect on N_0 and N_N and, as compared to the effect due to the variation of N_A , a negligible effect on b_A .

The values of N_0 , N_N , and b_A in Table VI give an excellent parametrization of our data. However, the values of N_0 differ from unity in a systematic manner, decreasing with increasing A . This implies that Eq. (4) is not adequate to describe the measured scattering distribution or that N_0 contains additional systematic errors not included in Table VI. Since N_0 and N_N are

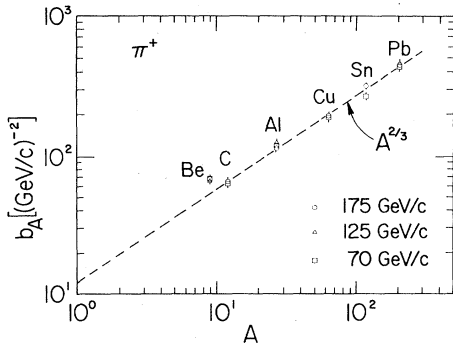


FIG. 10. Forward slope of coherent elastic scattering, b_A , versus target atomic weight A for π^+ . Fits for b_A were performed in the region of $0.0018 \leq -t \leq 0.0100$ $(\text{GeV}/c)^2$. Errors shown are statistical only (some errors not shown for presentation purposes). Dashed line has the form $A^{2/3}$ normalized to $b_A = 420$ at Pb.

highly correlated (the correlation coefficient between N_0 and N_N ranges from 0.93–0.98), we do not make the natural association of N_N with the total cross section for projectile nucleus scattering. Because of the correlation, we have assigned an additional uncertainty to the values of N_N . This uncertainty, which is substantial when N_0 is significantly different from 1.0, is given in the brackets in Table VI. Note that this uncertainty is not symmetric. We wish to point out that Eq. (4) assumes the nuclear t dependence is a simple exponential and ignores Coulomb nuclear interference effects. Either of the above could substantially effect our results for N_N and hence N_0 . The above statements do not apply to the determina-

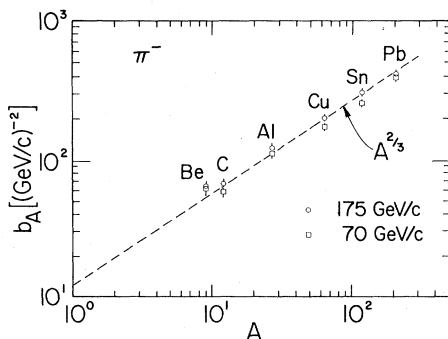


FIG. 11. Forward slope of coherent elastic scattering, b_A , versus target atomic weight A for π^- . Fits for b_A were performed in the region of $0.0018 \leq -t \leq 0.0100$ $(\text{GeV}/c)^2$. Errors shown are statistical only (some errors not shown for presentation purposes). Dashed line has the form $A^{2/3}$ normalized to $b_A = 420$ at Pb.

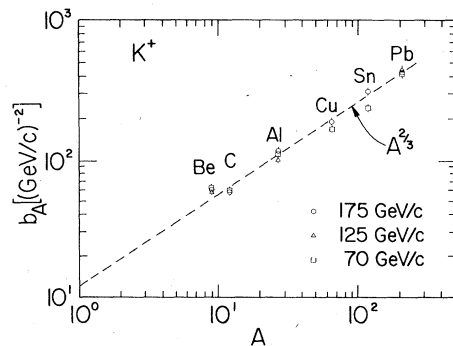


FIG. 12. Forward slope of coherent elastic scattering, b_A , versus target atomic weight A for K^+ . Fits for b_A were performed in the region of $0.0018 \leq t \leq 0.0100$ $(\text{GeV}/c)^2$. Errors shown are statistical only (some errors not shown for presentation purposes). Dashed line has the form $A^{2/3}$ normalized to $b_A = 410$ at Pb.

tion of b_A because b_A and N_0 are not highly correlated and the Coulomb nuclear interference term would only be important in the first few $-t$ bins.

Table VII presents values b_A derived from fits over approximately the same t region for all reactions. Figures 10–15 present the values found for the forward slope for coherent hadron-nucleus scattering (b_A) as a function of atomic weight. In general, for a given beam momentum and nuclear target, the forward slope is steepest when the incident projectile is a proton or antiproton and the shallowest when the incident projectile is a kaon.

The data for the Cu, Sn, and Pb targets were

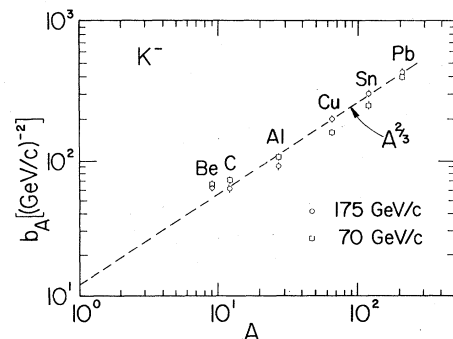


FIG. 13. Forward slope of coherent elastic scattering, b_A , versus target atomic weight A for K^- . Fits for b_A were performed in the region of $0.0018 \leq t \leq 0.0100$ $(\text{GeV}/c)^2$. Errors shown are statistical only (some errors not shown for presentation purposes). Dashed line has the form $A^{2/3}$ normalized to $b_A = 410$ at Pb.

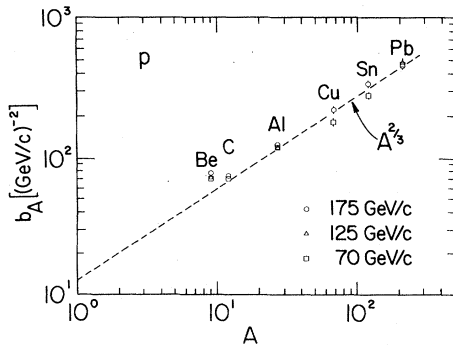


FIG. 14. Forward slope of coherent elastic scattering, b_A , versus target atomic weight A for p . Fits for b_A were performed in the region of $0.0018 \leq -t \leq 0.0100$ $(\text{GeV}/c)^2$. Errors shown are statistical only (some errors are shown for presentation purposes). Dashed line has the form $A^{2/3}$ normalized to $b_A = 450$ at Pb.

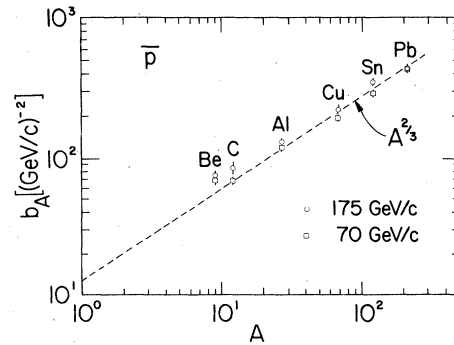


FIG. 15. Forward slope of coherent elastic scattering, b_A , versus target atomic weight A for \bar{p} . Fits for b_A were performed in the region of $0.0018 \leq -t \leq 0.0100$ $(\text{GeV}/c)^2$. Errors shown are statistical only (some errors not shown for presentation purposes). Dashed line has the form $A^{2/3}$ normalized to $b_A = 450$ at Pb.

fit substituting a Bessel-function form for the exponential in the coherent term of Eq. (4) in order to attempt to fit beyond the first minimum exhibited by these data. The fits resulted in a large χ^2 per degree of freedom which implies a more sophisticated theoretical treatment^{1,2} is necessary.

ACKNOWLEDGMENTS

We would like to thank the following people for their valuable contributions: Peter Martin, Sa-

tish Dhawan, Adrian Disco, Irving Winters, Jon Blomquist, Garvie Hale, and Ed Steigmeyer. We also thank William Frieze for his work on early parts of this experiment. This work was supported in part by the U. S. Department of Energy. One of us (L.R.) was a fellow of the Swiss National Fund for Scientific Research and a second member (L.A.F.) was supported in part by a Ford Foundation Doctoral Fellowship for Mexican-Americans and Puerto Ricans.

*Present address: Bell Laboratories, Holmdel, New Jersey 07733.

†Present address: Lawrence Berkeley Laboratory, Berkeley, California 94720.

‡Present address: CERN, Geneva, Switzerland.

§Visitor from Rutherford Laboratory, Chilton, Didcot, Berkshire, England.

||Present address: SLAC, P. O. Box. 4349, Stanford, California 94305.

¶Present address: Brookhaven National Laboratory, Upton, New York 11973.

**Present address: Arthur Young and Company, One IBM Plaza, Chicago, Illinois 60611.

¹R. J. Glauber and G. Matthiae, Nucl. Phys. **B21**, 135 (1970).

²A. S. Goldhaber and C. J. Joachain, Phys. Rev. **171**, 1566 (1968).

³G. Bellettini *et al.*, Nucl. Phys. **79**, 609 (1966).

⁴H. R. Blieden *et al.*, Phys. Rev. **D 11**, 14 (1975).

⁵V. D. Apokin *et al.*, Serpukhov Report No. Y2/A1-42 (unpublished).

⁶E. Jenkins *et al.*, submitted to the XIX International Conference on High Energy Physics, Tokyo, 1978 (unpublished); D. Gross *et al.*, Phys. Rev. Lett. **41**, 217 (1978).

⁷J. R. Orr and A. L. Read, Meson Laboratory, Preliminary Design Report, 1971, Fermilab (unpublished).

⁸J. Slaughter *et al.* (unpublished).

⁹A. Schiz *et al.*, Report No. FERMILAB-Pub-79/81-EXP (unpublished).

¹⁰W. Frieze *et al.*, Nucl. Instrum. Methods **136**, 93 (1976).

¹¹S. Dhawan and R. Majka, IEEE Trans. Nucl. Sci., **NS-22**, 303 (1975).

¹²Digital Equipment Corp., Maynard, Massachusetts.

¹³F. James and M. Roos, CERN Computer 7600 Interim Program Library, Nos. D506 and D516 (unpublished).

¹⁴H. A. Bethe, Phys. Rev. **89**, 1256 (1953). See, in particular, Eqs. (25), (27), (32), and (37). w is the width of the multiple-scattering Gaussian. β (B in Bethe's paper) is an expansion parameter that depends on the screening angle of the target nucleus and gives the relative contribution of higher-order terms in the full Bethe-Molière expression for Coulomb scattering. The values of w , in units of GeV/c , for the targets are 0.0031 (Be), 0.0034 (C), 0.0035 (Al), 0.0040 (Cu), 0.0047 (Sn), and 0.0038 (Pb). The values of β (dimensionless) for the targets are 12.03 (Be), 11.91 (C), 11.43 (Al), 11.08 (Cu), 10.77 (Sn), and 9.50 (Pb).

¹⁵ G_P and G_T were taken as follows: $G_P = (1 + (0.8)^2 q^2 / 12\hbar^2)^{-2}$, $G_T = \exp(q^2 R^2 / 6\hbar^2)$, where R is the electromagnetic radius of the target nucleus (see Table V for values of R used). It was found that if a monopole form for the form factor was used for the pions and kaons, there was negligible effect on the fit results.

¹⁶L. A. Fajardo, thesis, Yale University, 1980 (unpublished).

¹⁷A. Schiz, thesis, Yale University, 1979 (unpublished).

¹⁸The solid lines in Figs. 3–8 are calculated as follows:
The theoretical form of $d\sigma/dt$ is convoluted by the

acceptance and resolution of the apparatus. This convoluted form is then divided by the acceptance to get the fit results as shown in the figures. The fit results still exhibit effects of the apparatus resolution and therefore are not completely smooth.